International Journal of Applied Pharmaceutics

ISSN- 0975-7058 Vol 17, Issue 1, 2025

Original Article

OPTIMIZING ORAL BIOAVAILABILITY OF SUNITINIB: QUALITY BY DESIGN IN NANOBUBBLE FORMULATION

ANJANEYULU PATAMSETTI, KUMAR SHIVA GUBBIYAPPA*

Department of Pharmaceutics GITAM School of Pharmacy, GITAM Deemed to be University, Hyderabad-502329, Telangana, India
***Corresponding author: Kumar Shiva Gubbiyappa; *Email: sgubbiyappa@gitam.edu**

Received: 27 Aug 2024, Revised and Accepted: 18 Nov 2024

ABSTRACT

Objective: The use of dextran nanobubbles is aimed at function as a delivery system for drugs like sunitinib. These specially designed nanobubbles enhance the drug's solubility, stability, and bioavailability, thus improving the therapeutic effectiveness. Moreover, they offer controlled release characteristics and can potentially enhance drug delivery to tissues or cells, thereby maximizing pharmacological results while reducing adverse effects.

Methods: Drug-loaded dextran nanobubbles were formulated using the emulsification technique and optimized using a Box Behnken design that considered process and formulation parameters. The Nanobubbles characterization includes Particle Size (PS), drug loading, entrapment efficiency, Fourier Transform Infrared Spectroscopy (FTIR), Differential Scanning Calorimeter (DSC), X-ray diffraction studies, stability studies, and as well *in vitro* and *in vivo* studies in rats.

Results: The optimized nanobubbles displayed a PS of 177.8±5.2 nm, zeta potential of-21.1±0.43 mV, and poly dispersity index of 0.262±0.089. With 69.12±1.41% of entrapment efficiency and 26.29±4.01% drug loading, *in vitro* studies revealed a superior drug release (99%) with ultrasound versus plain drug (39%). FTIR and DSC studies confirmed no drug-polymer interaction. Scanning electron microscopy images displayed uniform spherical nanosized particles. Stability studies indicated no significant changes after 30 days. The nanobubbles exhibited increased C_{max} (4.52) and AUC_{0-t} (5.27), promising enhanced solubility, absorption, and extended half-life.

Conclusion: The current investigation shows that dextran nanobubbles loaded with sunitinib have a promising delayed release potential, which makes them a possible treatment alternative for cancer.

Keywords: Box-behnken design, Colorectal cancer, Dextran, Nanobubbles, Sunitinib, Sustained release, Soya lecithin, Palmitic acid

DOI: https://dx.doi.org/10.22159/ijap.2025v17i1.52462 Journal homepage: https://innovareacademics.in/journals/index.php/ijap

INTRODUCTION

Sunitinib, an oral multitargeted tyrosine kinase inhibitor, exhibits both antitumor and antiangiogenic effects by effectively targeting Vascular Endothelial Growth Factor Receptor (VEGFR) and other tyrosine kinases and c-kit receptor at nanomolar concentrations [1, 2].

Sunitinib, a novel inhibitor targeting the VEGFR, has shown remarkable effectiveness in the treatment of Renal Cell Carcinoma (RCC) and is currently extensively utilized for patients with advanced-stage cancer [3].

The bioavailability of sunitinib remains undisclosed. Absorption of sunitinib happens gradually, with T_{max} being noted between 6 to 12 h post-dosing. Sunitinib and its main metabolite (SU12662) demonstrate significant binding to plasma proteins in humans, with percentages of 95% and 90%, respectively [4]. It is also found to be highly effective for various solid tumors, including breast, colon and lung cancer [5, 6].

The drug is known to have low water solubility, leading to a slow dissolution rate and ultimately causing limited bioavailability when taken orally. Studies reported that in cancer patients, the peak concentration (maximum plasma concentration) of sunitinib in the bloodstream falls within a range of 20-30 ng/ml [7].

Also, the drug has an extended terminal half-life of 40-60 h means that it takes 2 w of consistent daily dosing to reach steady-state concentration [8]. Hence, it is imperative to develop efficient and secure sunitinib delivery mechanisms in order to enhance the localized drug concentration in the while reducing systemic exposure.

Different authors have employed various approaches to improve drug solubility by utilizing solid dispersion [9], Self-Nanoemulsifying Drug Delivery Systems (SNEDDS) [10], microspheres [11], polymeric nanoparticles, solubility improvement using carbondioxide (SC-CO_2) [12], micellar nano complex [13], and copper complex [14], have been by various authors to improve the *in vitro* dissolution rate and therapeutic effectiveness of sunitinib.

Despite advancements, achieving deep tissue penetration and effective drug distribution remains a challenge for some of the above approaches. Addressing these limitations through continued research and innovation is crucial to fully realize the therapeutic potential of quercetin in treating various diseases.

In addition to improving solubility, it is crucial to have a method that can direct drug molecules to diseased tissues while minimizing their presence in healthy tissues. The targeted delivery system will enhance the concentration of drug in the blood while improving the pharmacokinetics of the drug while reducing the side effects.

Nanobubbles are advanced nanoplatforms designed to enhance therapeutic treatments, featuring a spherical core-shell structure. These nanobubbles offer numerous benefits, including improved drug delivery efficiency, controlled release, altered pharmacokinetics and biodistribution, reduced dosage requirements, enhanced ability to overcome biological barriers, targeted delivery to specific cells, and minimized adverse effects. They have been extensively researched as delivery systems for drugs and nucleic acids, demonstrating effective oxygen storage capacity [15]. Additionally, nanobubbles are responsive to ultrasound, functioning as versatile nanocarriers. Their unique properties make them a promising tool in advanced medical treatments and drug delivery systems, offering the potential for significant improvements in therapeutic outcomes. Nanobubbles range in size from 500 nm to 1 nm.

To the best of our knowledge and based on the available literature, there are no prior studies documenting the utilization of dextran nanobubbles for delivering sunitinib. This research addresses a void in the field by utilizing dextran nanobubbles for sunitinib delivery

and implementing the Design of Experiments (DoE) for enhancement. DoE simplifies optimizing experimental variables through clear-cut strategies and statistical methods. The study involves designing, formulating, and optimizing drug-loaded Nanobubbles using dextran, followed by comprehensive *in vitro* and *in vivo* evaluation.

MATERIALS AND METHODS

Reagents and chemicals

Sunitinib is a pure drug given by Dr. Reddy's Laboratories, a private limited company in Hyderabad. Degussa (Hamburg, Germany) generously provided us with soybean lecithin (Epikuron 200®). C3F8 (Perfluoropropane) was procured from pharm affiliates Pvt ltd, Haryana, India. Sigma Aldrich, US, supplied Dextran, Epikuron®and palmitic acid. All other solvents were purchased from Qualigens, India.

Preparation of unloaded and drug-loaded nanobubbles

Nanobubbles were created by utilizing Perfluoropentane (PFP) as the inner core and dextran sulfate as the outer shell, following a multi-step procedure derived from prior studies. To produce empty Nanobubbles, a pre-emulsion was prepared by combining 400 µl** of an ethanol solution with 1% w/v Epikuron® and palmitic acid (0.5% w/v) with 500 µl** of PFP, while stirring magnetically at 800 rpm [19]. This mixture was then mixed with 5.0 ml of ultrapure water and homogenized using an Ultra-Turrax SG215 homogenizer for 3 min. Subsequently, 350 µl** of a 2.0 % w/v aqueous dextran sulfate solution (molecular weight 100 kDa) was added drop by drop with continuous magnetic stirring (800 rpm) for 3 h. The empty Nanobubbles were utilized as control formulations in the following experiments. To prepare drug-loaded Nanobubbles, a pre-emulsion was formed by combining 350 µl** of an ethanolic solution containing lipids and 9.8% w/v drug with 500 µl** of PFP. Following the introduction of ultrapure water, the blend was homogenized with an Ultra-Turrax homogenizer for duration of 3 min, then subjected to heating at 37 °C for a period of 15 min. Dextran sulfate (1.96 % w/v) was then added dropwise under gentle stirring conditions at 800 rpm. The resulting drug-loaded nanobubbles (Sunitinib-Nanobubbles) were purified through dialysis to eliminate unbound molecules. The nanobubbles were freeze-dried for 36 h and stored in vials with caps for further analysis [20].

The three independent variables were the amount of Dextran (w/v), amount of the drug (w/v) and homogenization speed (rpm), each at three levels of variation: low (-1), middle (0), and high (1). The response (four related variables) was Particle Size (PS; Y1), Polydispersity Index (PDI; Y2), Zeta Potential (ZP; Y3), and Encapsulation Efficiency (EE%; Y4); table 1 lists their respective ranges. The response surface search was conducted using Design Expert® tools (Version 12.0.3.0, Stat-Ease Inc., Minneapolis, MN), and response surface charts and contour (2D) plots were employed for analysis [21].

Table 1: **Factors influencing the experiment's design**

	Independent variables	**Levels**		
		LOW (-1)	**Medium (0)**	**High (+1)**
A	Amount of dextran (% w/v)	1.0	1.5	2.0
B	Drug concentration (%w/v)	8	10	12
C	Homogenization time(mins)	2	4	6
Dependent variables		*Restrictions*		
Y1	Particle size (nm)	Minimize		
Y2	Polydispersity index	Minimize		
Y3	Zeta potential (mV)	Maximum		
Y4	Encapsulation efficiency (%)	Maximum		

Characterization and evaluation

Measurements of PS, PDI, and ZP

By employing a Zeta-sizer (Malvern Instruments, UK), Dynamic Light Scattering (DLS) theory was used to calculate the PS, PDI, and ZP of Sunitinib Nanobubbles after tenfold dilution of the sample with double-distilled water [21].

EE

The EE of the drug in the nanobubbles can influence the therapeutic efficacy, stability, and release kinetics of the loaded compounds within the nanobubbles. Dichloromethane was used to dissolve a particular quantity of loaded drug-containing nanobubbles. The complex was dissolved by subjecting the solution to sonication for 10 min. The resultant solution was then suitably diluted and assessed for using the UV visible spectrophotometry ay 432 nm [20].

The following formulae can be used to calculate the same.

$$\%\ Drug\ Entrapment\ efficiency = \frac{Total\ amount\ of\ the\ drug - free\ drug}{amount\ of\ drug} \times 100$$

Morphology using scanning electron microscopy (SEM)

The nanobubbles and drug structure were imaged using a Quanta FESEM 250 SEM. Prior to testing; the sample underwent mounting on aluminum pin stubs, double-sided carbon tape mounting, and Au-sputter coating with the use of an ion splutter. The specimen was then analyzed at an operating distance of 10 millimeters, with an acceleration current of 30 kV and a magnification of 500–10,000 folds.

Fourier-transform infrared spectroscopy (FTIR)

The spectrum of FTIR was obtained using spectroscopy Perkin Elmer (Model 1600; USA). The pure drug, dextran, Physical Mixture (PM), and the optimized drug-loaded Nanobubbles were all analyzed at wave numbers 4000-450 cm^{-1} with a resolution of 1.0 cm^{-1} [11].

Differential scanning calorimetric (DSC) study and X-ray diffraction pattern (XRD)

The drug's physical structure and potential chemical interactions with excipients were determined using a DSC-60 (Shimadzu Corp., Japan). Samples weighing 3-5 mg (including pure drug, blank nanobubbles, dextran, and optimized drug-loaded nanobubbles) were heated (50-400 °C, 5 °C/min) in folded aluminum pans under a nitrogen atmosphere. Subsequently, DSC analysis was conducted after calibration with Indium and lead standards. The Melting Point (MP) and the enthalpy of fusion were computed automatically. The XRD patterns of pure drug, PM, and the optimized formulations were obtained using a Philips XRD (PW-1710) operational with a graphite monochromator and Ni-filtered Cu Kα radiation (at 100mV and 40kV). The samples were scanned between 2 and 80 degrees 2 theta (θ) angle from 2° to 60° with an average step size of 0.045° and a duration per step of 0.5 second [11].

Drug release (DR)

The release studies of pure drug and optimized drug-loaded dextran Nanobubbles were carried out through *in vitro* experiments using a shake flask equipped with a dialysis bag. Following encapsulation in dialysis membranes, the specimens were transferred into a conical flask containing phosphate buffer (pH 7.4), maintained at 37 °C, and subjected to constant rotation at 100 rpm. One milliliter sample was removed from the outer solution and replaced with brand-new PBS at

pH 6.8 at predefined intervals. These aliquots were filtered and analyzed using the UV visible spectrophotometer method at 432 nm to measure DR. Three duplicates of the experiment were carried out [13].

Stability studies

The stability of the optimized formulation was assessed by storing it at three different temperatures (4 °C, 25 °C, and 40 °C) under 75% relative humidity. Periodic measurements were taken to monitor alterations in PS, PDI, and EE of the samples [16].

High-performance liquid chromatography (HPLC) analysis

A reverse-phase HPLC with a C18-PM column (5 µm, 4.6 × 250 mm i. d., Hitachi, Japan) and a UV/Visible detector was used for chromatographic separation. The mobile phase consisted of a mixture of acetonitrile (with 1% formic acid) and 20 mmol ammonium formate in a 67.5:32.5 v/v ratio. The separation was carried out in isocratic mode at a flow rate of 0.75 ml/min, with samples (20 µl**) introduced and eluents detected at a UV absorbance of 431 nm [22].

Preparation of standards

The initial stock solution (1 mg/ml) was created through the measurement of the drug and erlotinib (internal standard). A calibration curve spanning from 10 to 500 ng/ml was produced using a secondary stock solution of 100 µg/ml.

Bioanalysis

The drug was isolated from plasma samples through the protein precipitation technique. A total of 250 µl** of acetonitrile was introduced to 50 µl** of rat plasma, and the solution was agitated. Subsequently, the combination underwent centrifugation at 8500 rpm for 10 min, and the resulting supernatant was assessed via chromatography at a λ_{max} of 431 nm [22].

Kinetic studies in animals

The male Wistar rats, with an average weight of 200±20 g and aged 4-5 w, were obtained from the Nutrition National Institute (NIN) in Telangana, India. The study followed the guidelines for the Care and Use of Laboratory Animals and received approval from the Institutional Animal Ethics Committee (IAEC) under protocol number 1447/PO/Re/S/11/CPCSEA-91/A. The animals were placed in natural light/dark cycles for a period of seven days, adjusting to a humidity level of 40–60% and a temperature range of 20ºC±2ºC. After that, they were randomly divided into two groups of six animals. The optimized drug-loaded nanobubbles (20 mg/kg BW) and the pure drug (dispersed in 0.5% w/v carboxymethylcellulose) were administered by oral route. The animal blood was obtained from the retroorbital plexus (300 µl**) and then transferred into sterile test tubes with Ethylenediaminetetraacetic Acid (EDTA) at specific intervals (1,2, 3, 4, 6, 8,10, 12, 16,20, 24, 36, and 48 h). Blood samples were centrifuged at 8500 rpm for ten minutes using an Eppendorf centrifuge. The plasma that was extracted underwent processing and analysis through HPLC following the method development outlined above. Non-compartmental analysis WinNonlin (version 3.1; Pharsight *et al.*, USA) was employed to calculate the C_{max} (Maximum Plasma Concentration), (AUC_{0-48}) area under plasma concentration *vs* time curve from 0 to 48 h, T_{max} (time to reach the maximum plasma concentration, K_{el} (elimination rate constant, $t_{1/2}$ (half-life). All the data were expressed as mean±SD.

RESULTS

Nanobubbles of sunitinib using dextran were developed using the emulsification technique successfully prepared using perfluoropentane as the core, with soya lecithin (Epikuron®) and palmitic acid forming a stabilizing lipid layer [23]. Dextran sulfate contains negatively charged sulfate groups, while sunitinib has amino groups that can be protonated (positively charged) depending on the pH, facilitating electrostatic interactions between the two. These opposite charges can enhance drug EE, control DR, and improve the stability of the nanobubble formulation. The effectiveness of these interactions is influenced by environmental pH, ionic strength of the solution, concentrations of both dextran sulfate and sunitinib, and the specific structural characteristics of the nanobubble shell [24].

The concentration of polymer, drug (A), and homogenization time were found to significantly influenced the PS, PDI, ZP, and entrapment of the Nanobubbles and hence were considered as Critical Quality Attribute (CQAs).

The QTPP (Quality Target Product Profiles) were clearly outlined in contrast to the traditional product and can be found in table 2. Qulaity by Design relies on the identification and precise monitoring of CQAs. Attaining QTPP is possible when CQAs are accurately defined and maintained within set limits.

The intention of nanobubbles was to increase the drug's stability, bioavailability, and biodistribution for targeted delivery to solve solubility problems, first-pass metabolism and to sustain the release. Nanoscale PS reduction can improve this, where PS, PDI, ZP, and EE were selected as critical quality attributes in the study. Table 2 offers a succinct summary of the chosen CQAs and an explanation.

Table 2: Selection of QTPP and CQAs and justification

QTPP	Target	Justification
Formulation	Nanobubble	The selected formulation strategy facilitates targeted drug distribution to the intended site of action while improving half-life, stability, and bioavailability.
Route of administration	Oral	The available formulation in the market is oral; hence, we are attempting to increase the half-life and bioavailability.
Drug release	More significant as compared to PD	Decreased size can improve the rate of drug release.
Stability	Up to thirty days following formulation, no outward indications of aggregation or cake formation	Because particle size affects this formulation's efficiency, it is critical to keep it constant.
CQAs		
CQA	Target	Justification
Particle size	In Nano-range	Reducing the size of the nanoscale increases surface area, which boosts release and distribution to the site.
Polydispersity index	Should be less than 0.3	Less than 0.3 helps the formulation to be homogenous rather than heterogeneous
Zeta Potential	In range-23.0 to 25.0 mV	It should be in range as it helps in the stability of the formed nanobubbles
Entrapment efficiency	High	A high EE helps to release the drug at the site and also reduces the dose of the drug and its related side effects

We utilized a three-factor, three-level Box-Behnken design in our research, consisting of seventeen runs, including three replicates at the center points. The outcomes of the randomized trials, which include the selected independent and dependent variables, are outlined in table 3.

We employed 2FI multiple linear regression analysis to construct polynomial models encompassing quadratic, two-factor, and linear models. The model selection process involved the use of R^2, predicted R^2, adjusted R^2, and Coefficient of Variance (C. V).

Table 3: Runs designed for the trails

Run	Factor A	Factor B	Factor C	Response Y1	Response Y2	Response Y3	Response Y3
	A: Amount of dextran	B: Drug concentration	C: HS	Particle size	Polydispersity index	Zeta potential	Encapsulation efficiency
	% w/v	% w/v	rpm	nm		mV	%
1	1	8	4	226.3	0.318	-18.43	55.47
2	2	10	4	174.7	0.184	-21.94	64.08
3	2	12	6	228.44	0.228	-18.28	44.41
4	2	10	4	180.5	0.123	-21.78	68.1
5	3	8	4	201.89	0.219	-26.88	74.76
6	3	12	4	159.64	0.122	-20.88	31.04
7	2	10	4	179.26	0.154	-21.05	68.88
8	2	12	2	177.12	0.192	-22.22	32.26
9	3	10	6	204.4	0.139	-26.66	67.16
10	3	10	2	214.12	0.162	-19.8	45.07
11	1	12	4	248.8	0.398	-22.98	53.25
12	1	10	2	262.88	0.326	-26.46	60.03
13	1	10	6	224	0.341	-13.86	61.69
14	2	10	4	179.1	0.149	-23.61	74.77
15	2	8	2	262.03	0.24	-21.89	62.94
16	2	8	6	169.2	0.252	-23.69	64.32
17	2	10	4	152.78	0.212	-22.69	68.84

The nanobubble size (Y1) and PDI (Y2) ranged from 152.78 nm to 262.28 nm, and 0.122 to 0.398; while the ZP (Y3) ranged from-26.88 mV to-13.86 mV. Likewise, the EE (Y4) ranged from 31.04 % to 74.77 % across all the trails.

PS

The small size of Nanobubbles results in a significantly higher surface area-to-volume ratio, enhancing their stability, penetrability, and reactivity in targeted drug [25].

The model F value (18.02), indicating only a 0.05 percent chance of being due to noise, suggests that the proposed model is quadratic and noteworthy, with an insignificant lack of fit. The Surface Response (SR) and Contour Plots (CP) displaying the impact of various variables on PS is displayed in fig. 1, and the perturbation plot of all variables is shown in supplementary fig. 1**.** The "lack of fit F-Value" (0.65) indicates that any lack of fit is not statistically significant relative to the pure error. There is 62.21 % chance that a "Lack of Fit F-value" of this magnitude would arise due to random noise, underscoring the model's reliability. ANOVA revealed that variables with p-values below 0.0500 significantly influenced the response. The R^2, adjusted R^2, and predicted R^2 were 0.9586, 0.9054, and 0.7391, respectively. The model adequately explored the design space with a precision of 12.492, exceeding the necessary threshold of 4. The model terms A, C, AB, BC, CD, A^2, and C^2 had a significant impact on the outcome. The variables are currently considered significant, leading to the following regression equation:

$$Particle\ Size(PS) = +173.27 - 22.74A - 5.68B - 11.26C - 16.19AB + 7.29AC + 36.04BC + 26.529A^2 + 9.37B^2 + 26.56C^2$$

The quadratic equation for PS describes the influences of variables A, B, and C on PS. This model shows that increases in A, B and C individually decrease PS, with A having the most significant linear effect. The interaction terms reveal that while AB reduces PS, AC and BC increase it, highlighting the complex interplay between these factors. The quadratic terms indicate that higher levels of A and C lead to substantial increases in PS, suggesting non-linear effects.

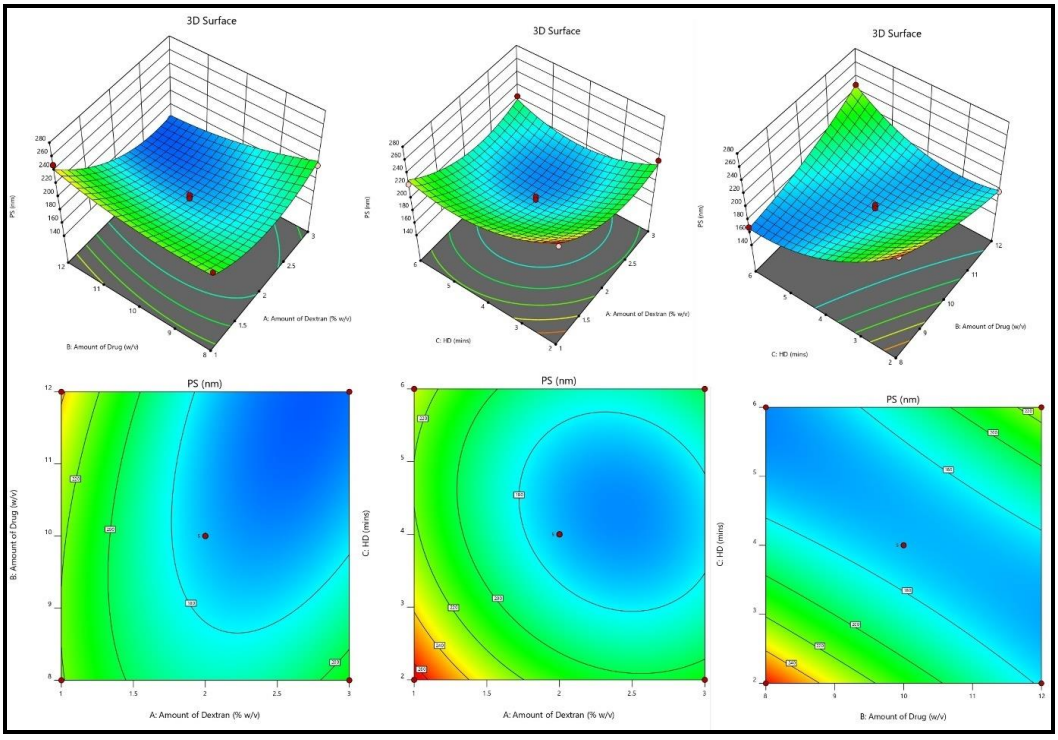

Fig. 1: Response surface and contour plots illustrating variable effects on particle size (PS)

PDI

The PDI is a dimensionless measure of the broadness of the PS distribution, typically ranging between 0 an PDI d 1. PDI ranging from 0.122 to 0.398 were observed in the developed formulations [25]. The F value of 14.68 suggests a minor lack of fit for the proposed quadratic model, which was found to be statistically significant. Lack of fit, statistically insignificant based only on pure error, yielded an F-value of 0.22. There is 87.75 percent chance that a Lack of Fit F-value this large could be due to noise. ANOVA identified significant factors (p-value<0.0500), with non-significant variables removed to refine the model. The regression coefficients for R^2, adjusted R^2, and anticipated R^2 were 0.9497, 0.8850, and 0.8181, respectively. The model proved to be effective in exploring the design space, showing a precision of 12.745, which exceeded the required threshold of 4.

The model coefficients for terms A, AB, A^2 and B^2 were found to have p-values below 0.050, signifying a significant influence on the result. As a result, these variables are considered essential, leading to the following regression equation:

$$Polydispersity\ index\ (PDI) = +0.1644 - 0.0926A - 0.0111B + 0.0050C - 0.0443AB - 0.0095AC + 0.0060BC + 0.0569A^2 + 0.0429B^2 + 0.02076C^2$$

The equation indicates that increases an in A and B contribute to decreasing PDI due to the negative coefficients of the linear terms, suggesting that higher levels of these variables improve the homogeneity of the formulation. Conversely, C slightly increases PDI as indicated by its positive linear term, implying that higher levels of C may reduce uniformity. Interaction terms AB and AC both show negative coefficients, leading to a decrease in PDI, while the BC interaction slightly increases PDI. The quadratic terms A^2, B^2, and C^2 all have positive coefficients, indicating that higher levels of any of these variables result in increased PDI, demonstrating non-linear contributions to variability in PS distribution.

The 3D and Response surface plots are shown in fig. 2 demonstrate that homogenization speed significantly influences PDI. Despite all formulations maintaining PDI within acceptable bounds, below 0.3, higher stirring speed of the polymer to cross-linker at a lower molar concentration led to a slight increase in PDI. Initially, faster stirring improves monodispersity by enhancing particle uniformity. However, excessive stirring can increase the energy imparted to the particles, reducing their repulsive forces and leading to agglomeration. This observation correlates with PS expansion exceeding optimal homogenization.

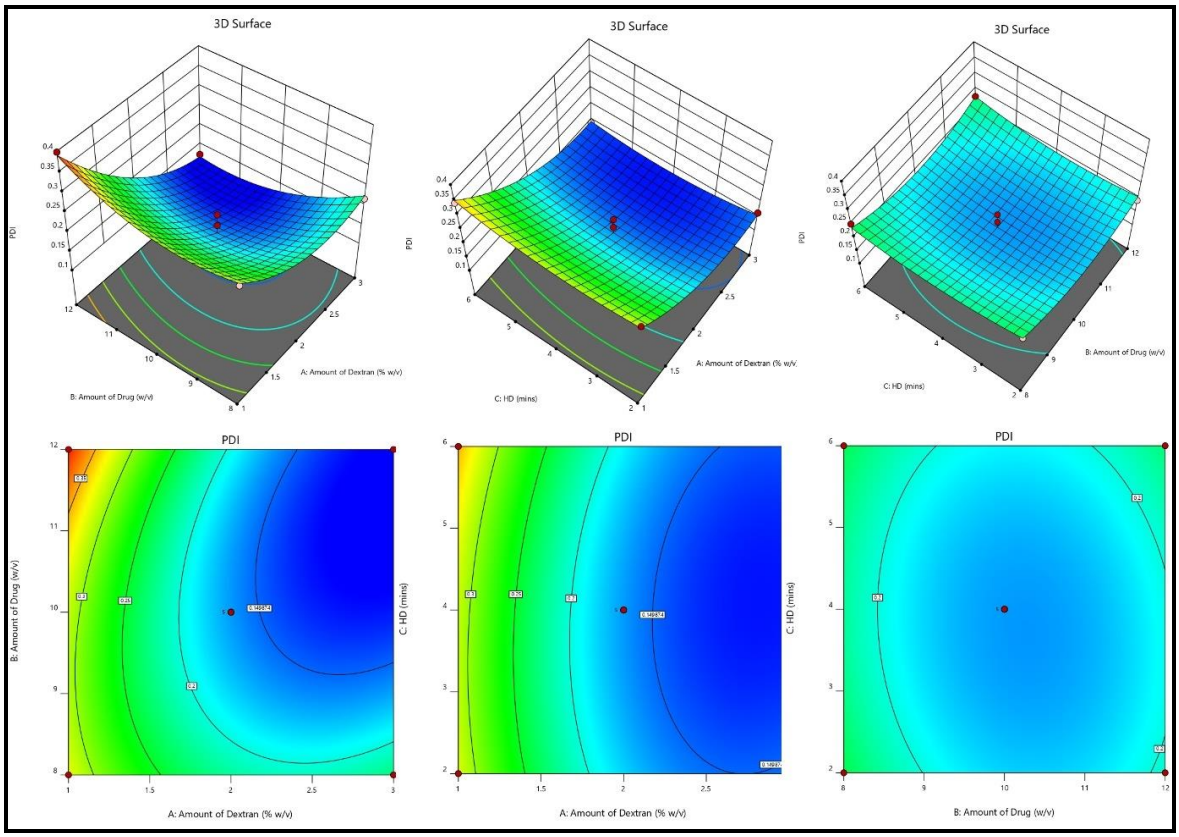

Fig. 2: Surface response and 3D plots depicting the effect of variables on PDI

ZP

It is influenced by surface charges shows an important role in the stability of nanoparticles suspension and the initial interaction of nanoparticles with cell membrane, making it crucial for effective drug delivery [25, 26]. In our study, the ZP of nanobubbles ranged from-26.88 mV to – 13.86 mV. The quadratic model for ZP demonstrates notable statistical significance, illustrated by the substantial F-value of 30.64. Regression coefficients (R^2, adjusted R^2, and anticipated R^2) were 0.9484, 0.9175, and 0.8316, respectively. The predicted R^2 aligns closely with the adequate R^2, differing by 0.2. The model, evidenced by adequate precision (signal-to-noise ratio) of 21.25, surpassing the necessary value of 4, proved useful for exploring the design space. Each individual variables (A, B, and C), interactive terms (AB, AC, BC) have a substantial effect on ZP, with P value below 0.0500 for all of them. The F-value for lack of fit (0.89) suggests that there is no statistically significant lack of fit. With a 57.09% probability that a lack of fit F-value of this level could be attributed to random variation, the model's dependability is confirmed. A lack of fit that is not statistically significant is preferred as it signifies a well-fitted model. Hence, these terms are deemed essential, leading to the following regression equation.

$$Zeta\ Potential(ZP) = -21.95 - 1.56A + 0.8162B + 0.9850C + 2.64AB - 4.87AC + 1.43BC$$

Positive coefficients signify a positive correlation, showing that as the variable(s) in question increase, ZP also increases. On the other hand, negative coefficients indicate a negative correlation, meaning that a decrease in the related variable(s) leads to a decrease in ZP. In this model, the ZP decreases with increasing values of A as indicated by the negative coefficient (-1.56), suggesting that higher levels of A reduce the stability of the colloidal system. On the other hand, increases in B and C lead to higher ZP, as shown by their positive coefficients of 0.8162 for B and 0.9850 for C, indicating improved stability with these factors. Among the interaction terms, AB and BC positively impact ZP with coefficients of 2.64 and 1.43, respectively, enhancing stability when both factors are present. Conversely, the AC interaction has a negative coefficient (-4.87), which decreases ZP, suggesting a potential reduction in stability when both factors are increased together. Overall, A decreases ZP, while B, C, and interactions AB and BC increase it, with AC leading to a reduction in ZP. The SR and CP demonstrating the consequence of variables on ZP is shown in fig. 3.

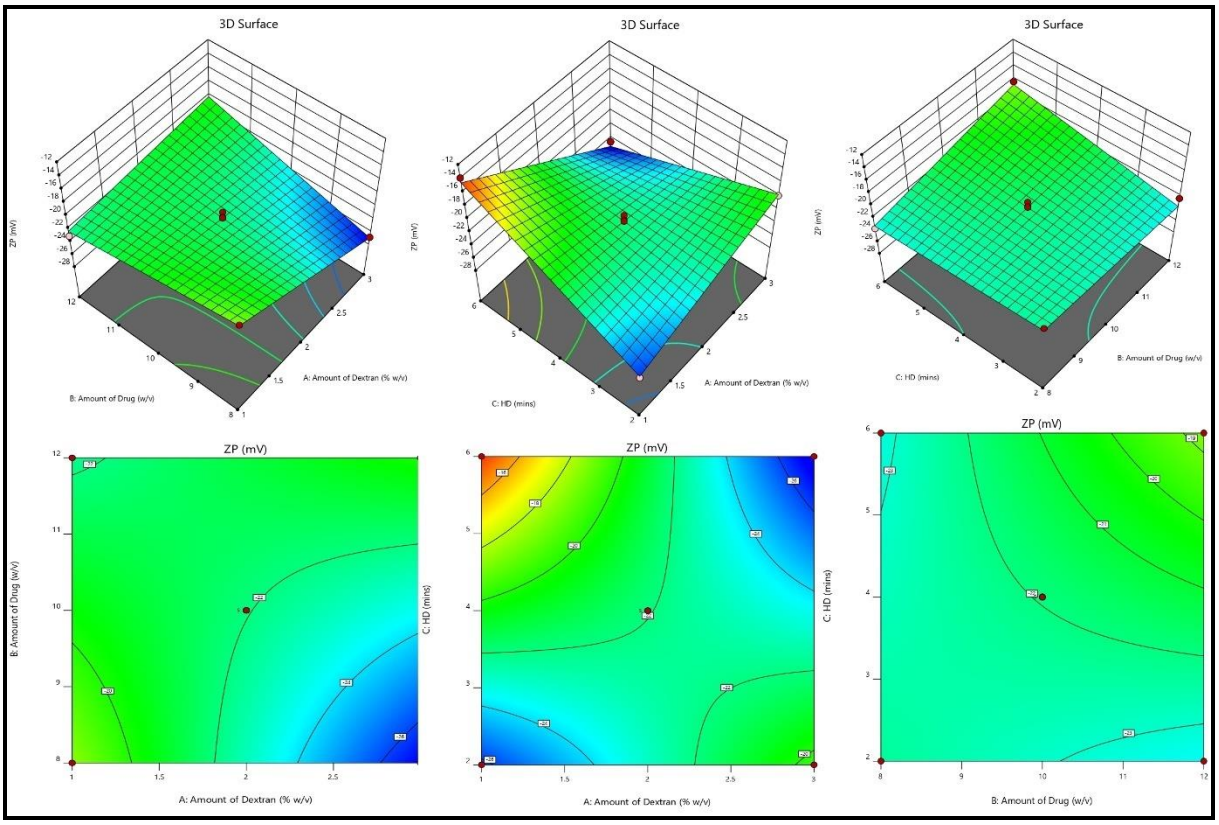

Fig. 3: Graphical representation of SR and contour plots (CP) demonstrating the consequence of variables on ZP

EE

Impact on EE ranges from 74.77 to 31.04%. The nanobubbles with high entrapment is always desirable to reduce the dose of the drug. The model's F value (27.27), with a probability of 0.01%, suggests significance and minimal fit error for the proposed quadratic model, likely not attributable to noise. The lack of fit's F-value (0.48) is n't statistically significant based on pure error, with a 71.16% probability of being noise. ANOVA identified significant factors (p-value<0.0500), leading to removal of non-significant variables. In fig. 4, you can see the response surface and contour plots that demonstrate the impact of variables on EE. The regression coefficients, such as R^2, adjusted R^2, and predicted R^2, were calculated at 0.9723, 0.9366, and 0.84501, respectively. The predicted R^2 is very close to the adequate R^2, with a difference of just 0.2. The model exhibited satisfactory accuracy with a signal-to-noise ratio of 17.3667, surpassing the minimum threshold of 4, showcasing its effectiveness in investigating the design space. Key model terms such as B, C, D, AB, AC, A^2, B^2, and C^2 displayed notable impacts with p-values<0.050. The resultant regression equation can be expressed as:

$$Entrapment\ efficiency\ (EE) = +68.93 - 1.55A - 12.07B - 4.66C - 10.38AB + 5.11AC + 2.69BC - 3.90A^2 - 11.40B^2 - 6.55C^2$$

This equation reveals that EE is affected by variables A, B, and C as well as their interactions. Specifically, increasing A and B leads to a decrease in EE due to their negative linear coefficients; conversely, increasing C enhances EE, as indicated by its positive linear coefficient. Among the interaction terms, AB has a negative coefficient, suggesting that the combination of A and, B decreases EE. In contrast, the interactions AC, and BC show positive coefficients for AC and BC, indicating that these combinations increase EE. Additionally, the quadratic terms for A^2, B^2, and C^2 are negative, demonstrating that higher levels of each factor individually lead to a decrease in EE.

Optimal preparation for exploration

The Derringers desirability technique was applied to optimize the variables affecting response parameters. This involved transforming response into a desirability scale, amalgamating them into a geometric mean function through exhaustive searches, ultimately yielding a global desirability value. The optimum configuration (F opt solution) with drug is 9.835 % w/v, dextran at 1.967 %, at a homogenization duration of 4.8 min resulted in a D value of 0.704. By adjusting the specified values for CQAs like PS, PDI, ZP, and EE, we were able to improve the potential for customized graphics. The design space and overlay plot are shown in fig. 5. Three checkpoints were used for validation to confirm the model's strength and formulation. As signaled in supp. Table 1, the anticipated mean values for size were 172.96 nm, with a PDI of 0.173, with a ZP of-21.549 and EE of 70.533, correspondingly, while the detected mean values were found to be 177.8±5.2 nm, 0.262±0.089, ZP of-21.1± 0.43 and EE of 69.12±1.41.

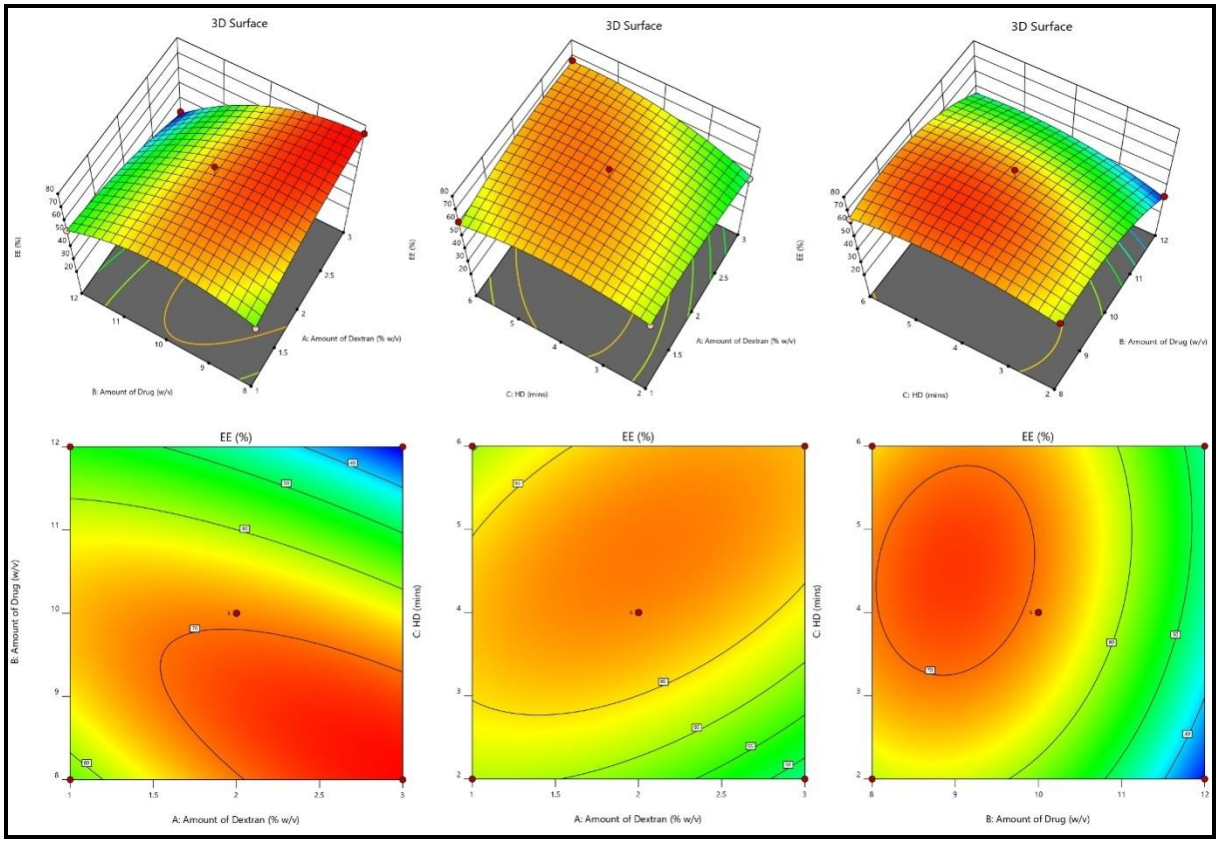

Fig. 4: Graphical representation of SR and contour plots (CP) demonstrating the consequence of variables on EE

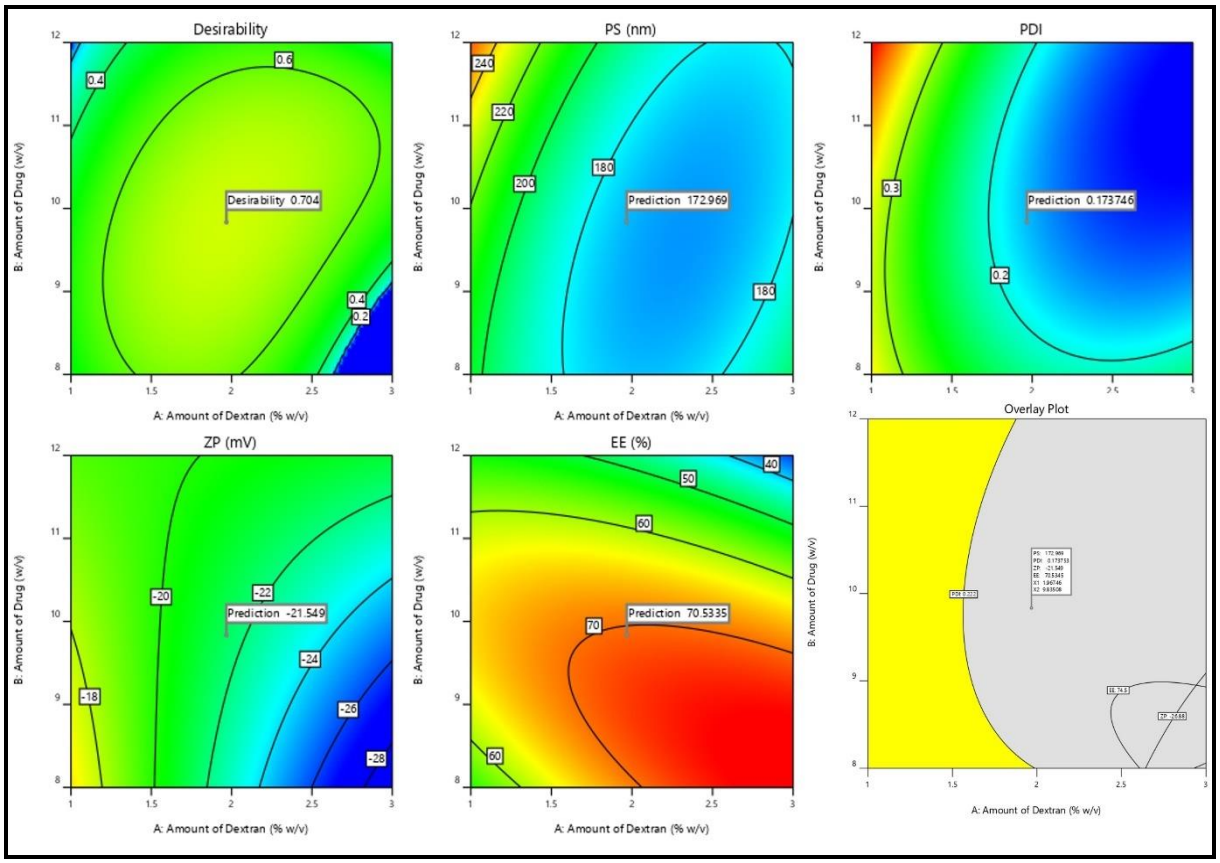

Fig. 5: Graphical illustration of desirability and overlay plot (Grey area denoted feasible region)

Evaluation

PS, ZP, and EE

The nanobubbles displayed consistent size and uniformity, as evidenced by the PS of 177.8±5.2 nm and PDI of 0.262±0.089, indicating a homogeneous system (PDI<0.3). The ZP of the optimized formulation was found to be-21.1±0.43 mV, highlighting the stabilizing effect of steric stabilizers surrounding the particles, which is essential for stability based on the double electric layer (DEL) theory. EE was calculated to be 69.12±1.41%, with a drug loading of 25.13±2.60%. Fig. 6 provides a visual representation of the PS, PDI, and ZP [27].

SEM

Fig. 6 depicts the surface properties of the formulation and the drug. The drug in its initial state, displays a broad range of PSs and irregular cubic shapes with micrometer-sized particles. Conversely, when the drug is transformed into nanobubbles, it produces spherical nanoparticles consistently measuring below 200 nm, as verified by the zeta sizer. This research showcases the successful achievement of nanosizing the drug through nanobubble formation, resulting in particles within the nanometer scale and exhibiting a low PDI [19].

FTIR

Analyzing the nanoformulation, excipients, and simple sunitinib IR spectra was used to determine component compatibility, as shown in fig. 7. 400–4000 cm^{-1} was the scanning range used. The basic medication exhibited clear peaks at (1743.71, 1687.77, 1498.74, 1309.71, and 1244.13 cm^{-1}), which correspond to C=C–F, C=O stretching of amide, C=C stretching of an aromatic ring, and C–N bending and P=O stretching. The N–H bending vibration mode was observed at 1510.31 cm^{-1}. In the case of dextran, it shows distinct peaks at (2926.11, 1610.61, 1157.33, 1078.24, 916.22 and 1321. 28) corresponding to OH stretching vibrations, CH stretching, bound water, C-O-C glycosidic bond stretching, C-O stretch of pyranose ring, glycosidic linkage and also CH bending. As no new peaks were seen in the Nanobubbles preparation and PM it clearly indicates no chemical interaction between the stabilizer and medication [16].

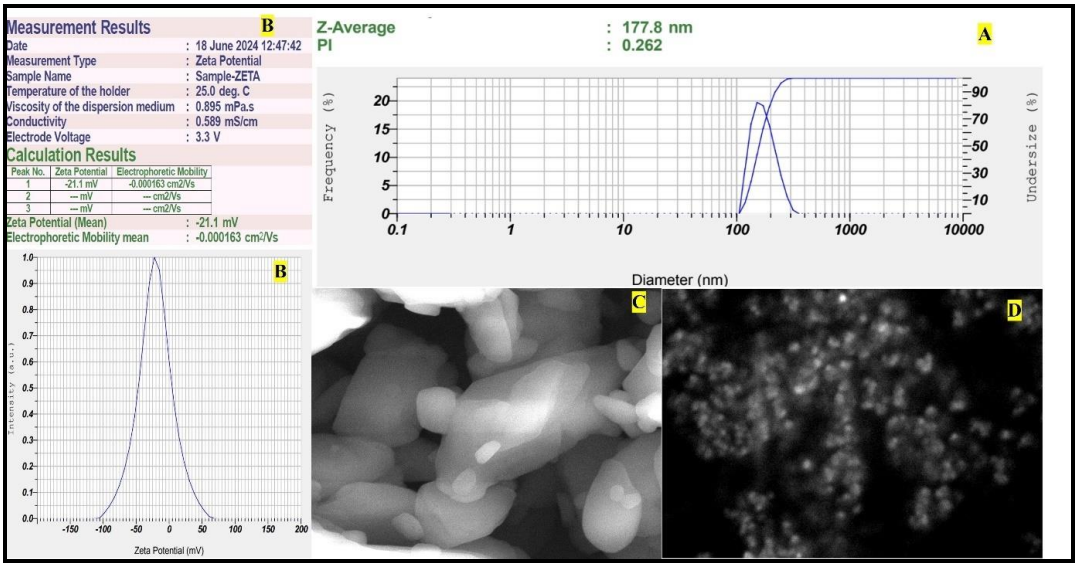

Fig. 6: Malvern image of A) Particle size and PdI; B) ZP; C) SEM image of pure drug; D) nanobubbles (Nanobubbles)

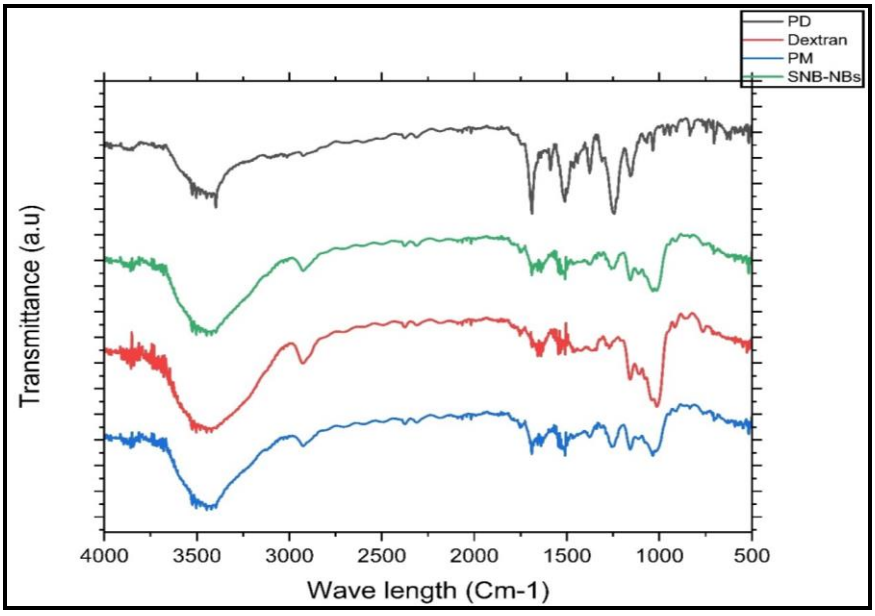

Fig. 7: A) Overlay of FTIR analysis A: Sunitinib-PD (black line-pure drug); B: Dextran (red line-); C: Physical mixture-PM (Blue line); D) Formulation nanobubbles (green line)

DSC and XRD

DSC assessment was accomplished to evaluate the thermal characteristics of the drug, dextran, and the nanobubbles (fig. 8). The pure drug exhibited a clear endothermic peak at 217.97 °C, signifying its melting point, indicating its crystalline characteristics.

The thermograph of dextran exhibited peaks at 295.6 °C. In the thermographs PM peak is seen at 145.71 °C. In the optimized nanobubbles, two prominent peaks emerged at 205.59 °C and 236.10 °C indicate a minor shift in the MP of the drug and its confinement within the polymeric structure due to weak intermolecular interactions between the drug and the polymer [28]. The XRD patterns are depicted in fig. 6B. The drug has displayed firm diffraction peaks (2θ scattered angles of 13.98, 14.78, 15.62, 17.26, 21.01, 22.7, 24.3, and 27.88°) confirming its crystalline nature. Previous studies have also reported similar diffraction peaks for the drug under study. However, in the nanobubbles, the characteristic diffraction peaks of drug vanished, suggesting the pure drug may have formed a solid-state complex at a molecular level in the nanobubbles [27].

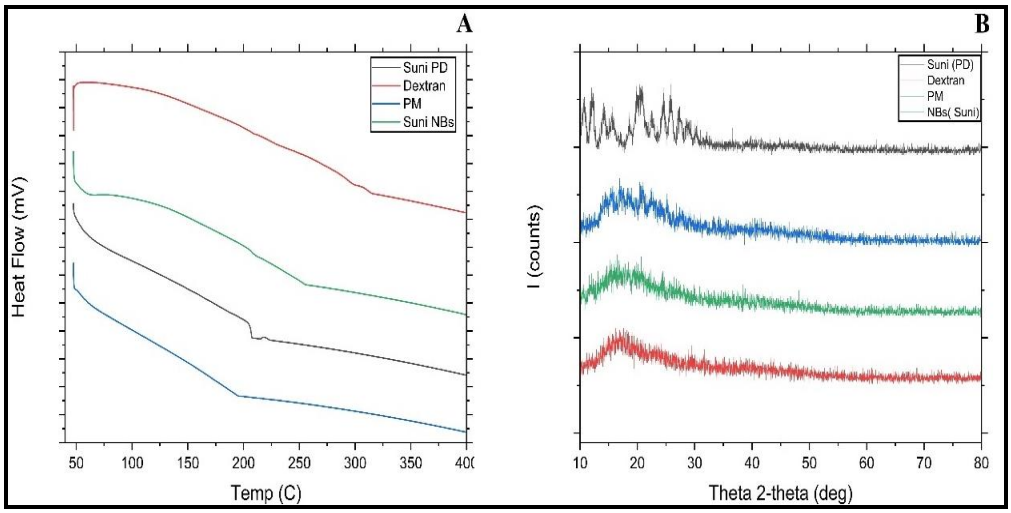

Fig. 8: A) Overlay of DSC thermograms of i) Suni-PD (black line); ii) Dextran (red line); iii) PM-physical mixture (blue line); iv) Formulation (optimized Nanobubbles green line); B) Overlay of XRD of i) Suni-PD (black line); ii) Dextran (red line); iii) PM (blue line), iv) Formulation-nanobubbles (Green line)

DR

Fig. 9 depicts dissolution profiles of plain drug and drug-loaded nanobubbles without and with acoustic assistance. DR from nanobubbles was significantly higher than a simple drug suspension. Notably, ultrasound assistance increased DR. The Cumulative Drug Release (CDR) at 8 h was 12.22±2.24%, 22.18±4.2%, and 38.68±6.1 % for plain drug, nanobubbles without acoustic, and with acoustic, respectively. By 40 h, over 94.81±8.47% was released from nanobubbles with acoustic assistance and 64.89±8.26% without acoustic, but in the case of the pure drug, only 34.34±4.60% of the drug was released. DR occurred due to collapse cavitation induced by acoustic waves, disrupting nanobubble structures and enabling rapid medication release. Acoustic waves, with meticulous control and non-invasive nature, offer accurate drug delivery and targeting abilities. These findings confirm that ultrasound assistance plays a pivotal role in enhancing DR from the nanobubbles potentially through the cavitation effect induced by ultrasound. Ultrasound stability studies indicated the transformation of the gas core from nanodroplets to bubbles, known as acoustic droplet generation. Under the influence of ultrasound, the oscillation of bubbles can trigger the shell to open, thereby aiding in the release of drugs. The study aligned with previous findings on nanobubble stability under varying temperature conditions. The acoustic streaming flow generated by bubble oscillation regulates the movement of detached materials, which is influenced by both the radial excursion and the duration of the ultrasound pulse [18].

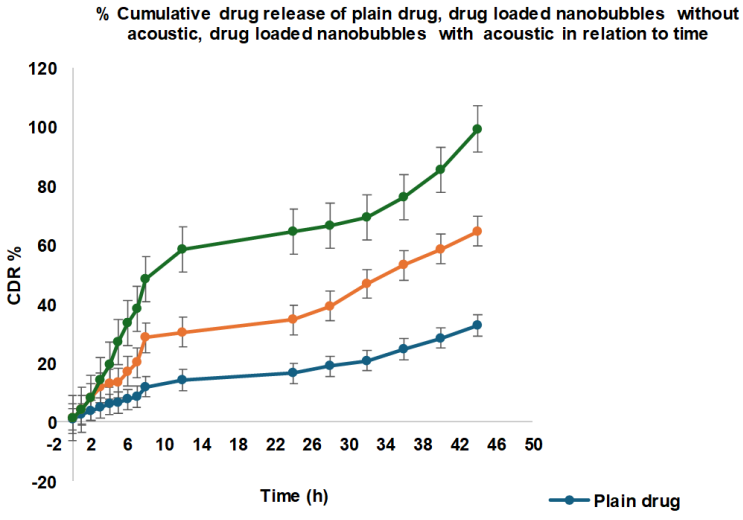

Fig. 9: *In vitro* drug release of plain drug, drug-loaded nanobubbles with and without ultrasound aid, all the values were expressed in mean±SD (n=3)

Stability studies

Sunitinib-loaded Nanobubbles underwent stability assessments at various storage conditions (4 °C, 25 °C, and 40 °C) for 0, 1 mo, two months, and three months (table 4). At 4 °C and 25 °C, minimal changes in drug content indicated robustness, with EE showing slight variation, suggesting protection against degradation. However, a notable reduction in EE occurred at elevated temperatures, where EE was reduced to 61.10±3.60 % from 69.12±1.41%, indicating structural disruption. Throughout the experiment, the PS of the formulation is less than 200 nm, and the ZP is around-21.2± 2.36mV, highlighting the stability and uniformity of sunitinib nanobubbles. Storage in a polyethylene pouch led to a faster drop in number concentration compared to a glass bottle. Hydrogen bonding interactions were emphasized as critical factors in forming bulk nanobubbles and their exceptional long-lasting stability [19].

Pharmacokinetic studies

Fig. 10 displays the plasma concentration-time curve after drug administration in 0.5% w/v carboxymethylcellulose solution and the optimized nanobubbles orally. Pharmacokinetic data in table 5 reveal that the formulation exhibited significantly higher T_{max}, C_{max} (**p<0.001), Area under the curve AUC_{0-24} (**p<0.001), and AUC0-∞ (**p<0.001) values compared to the pure drug suspension at the prescribed dose. The bioanalytical chromatogram indicated drug retention time at 8.4 min and, internal standard (erlotinib) at 6.2 min and the plasma peak at 3.5 min respectively (suppl. fig. 2).

The optimized formulation reached a maximum level (C_{max}) of 4.52 times higher, while the AUC_{0-t} was 5.27 times higher than the free drug. *In vivo* studies revealed a progressive DR from the nanobubble preparation with an extended half-life. Comparing the data to the free drug, oral bioavailability has significantly improved. This finding suggests a notable improvement in oral bioavailability compared to the free drug. The enhanced bioavailability can be attributed to the increased drug circulation at the nanoscale and the improved penetration facilitated by the polymeric carrier system.

Table 4: Stability data of the nanobubbles stored at various temperatures

Temperature	Months	PS (nm)	PDI	EE (%)
5±3 °C	Initial	177.8±5.2	0.262±0.089	69.12±1.41
	0.5	176.16±6.04	0.266±0.057	69.0±1.65
	1	177.9±7.22	0.268± 0.044	68.09±3.92
	2	178.48±5.04	0.263±0.034	68.16±3.30
	3	181.26±6.34	0.264±0.037	67.19±3.66
25±2 °C	Initial	177.8±5.2	0.262± 0.089	69.12±1.41
	0.5	178.26±2.16	0.279±0.066	69.02±2.85
	1	179.40±2.28	0.294±0.010	68.83±4.60
	2	180.68±4.98	0.280±0.041	67.37±2.89
	3	182.33±5.48	0.276±0.064	66.01±3.58
40±2 °C	Initial	177.8±5.2	0.262±0.089	69.12±1.41
	0.5	180.35±6.26	0.269±0.088	65.58±2.81
	1	182.13 ±4.06	0.298±0.032	63.22±2.16
	2	185.47±4.70	0.286±0.038	62.79±3.38
	3	184.26±6.52	0.296±0.046	61.10±3.60

All the values were expressed in mean±SD (n=3)

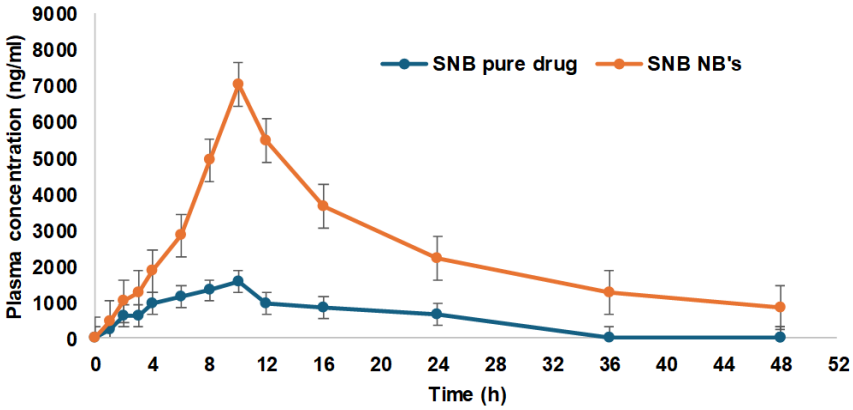

Fig. 10: *In vivo* pharmacokinetic studies, all the values were expressed in mean±SD (n=3)

Table 5: Pharmacokinetic parameters

Pharmacokinetic parameters	Pure drug	Drug loaded nanobubbles
C_{max} (ng/ml)	1560.47± 135.88	7061.20± 262.63
T_{max} (h)	8	10
Half-life (h)	6.39± 1.66	15.86± 2.35
AUC 0-t (ng. h/ml)	20252.5± 474.28	106814.06± 809.94
AUC 0-inf (ng. h/ml)	22857.75± 649.28	120380.29± 757.31
Ke (h^{-1})	0.108	0.0436
MRT(h)	12.85± 3.08	23.62±5.48

All the values were expressed in mean±SD (n=3)

DISCUSSION

In this study, sunitinib-loaded dextran nanobubbles were formulated using the emulsion method, with optimization conducted through the Box Behnken design. Nanobubbles are emerging as a formulation strategy because of their targeting ability.

Perfluoropentane undergoes a phase transition that turns nanodroplets into nanobubbles with high ultrasonic wave reflectivity. The echogenic qualities of perfluoro pentane make them visible in ultrasonography images [29]. The Nanobubbles were developed using dextran polymer containing unbound carboxylic end chains using perfluoro pentane for the inner core and poly(lactic-co-glycolic) acid as the outer shell [30]. The term "ultrasound" describes mechanical vibrations or pressure waves that exhibit compressional and rarefactional pressure fluctuations and have frequencies equivalent to or higher than the human hearing threshold (20 kHz) [15].

Ultrasound effects primarily involve two mechanisms: cavitation and sonoporation. The cavitation effect plays a crucial role in reducing the size of bubbles, whereas the sonoporation effect facilitates the uptake of these reduced bubbles [32]. Combining ultrasound with nanobubbles helps in drug localization while overcoming the off-target adverse effects. The nanobubbles using dextran have garnered attention for targeted drug delivery because of their unique physical and surface properties [33]. Dextran is highly recommended in various medical applications, including bone implants and sustained DR systems, due to its biocompatibility and biodegradability properties [34].

The quadratic model suggested by the design was applied to PS, PDI, ZP, and EE. Positive coefficients in the model indicated a positive connection, signifying that an increase in associated variables led to higher drug entrapment. Stabilizer concentration has affected PS, PdI, and ZP. However, when it came to EE, a high stabilizer concentration led to a decrease in drug entrapment. Dextran, as a polymer along with lipid stabilizers, has the potential to impede drug entrapment in nanobubbles due to its competition for surface adsorption and the subsequent increase in solution viscosity.

FTIR studies confirmed compatibility between drug and excipients. DSC and XRD studies revealed no distinct drug peak in the formulation, indicating the absence of crystalline drug material [12].

SEM analysis displayed homogeneous, smooth, spherical-shaped nanobubbles. DR occurred due to collapse cavitation induced by acoustic waves, disrupting nanobubble structures and enabling rapid medication release. Ultrasound stability studies indicated the transformation of the gas core from nanodroplets to bubbles, known as acoustic droplet generation [11].

The study aligned with previous findings on nanobubble stability under varying temperature conditions. The temperature-dependent behavior observed in PS, ZP, and entrapment emphasized understanding nanobubble characteristics in diverse environmental conditions for practical drug delivery applications. Different polymer materials submerged in nanobubble dispersions exhibited varied effects on Nanobubble number concentrations due to hydrophobic interactions. *In vivo* studies in Wistar rats revealed gradual DR from the formulation, leading to an increased half-life of the drug with high AUC. These findings indicated a significant improvement in the oral bioavailability of the chosen medicine using nanobubbles compared to free drug [35]. The improved bioavailability of nanobubbles with dextran is achieved through various mechanisms. These include better drug encapsulation within dextran nanodroplet, longer circulation time due to the protective coating of dextran, and increased uptake by target cells or tissue.

CONCLUSION

This research introduces an innovative approach to improving the solubility of sunitinib nanobubbles. By conducting a thorough investigation, the study demonstrates that nanobubbles significantly enhance the release of drug, indicating their potential as a new and smart delivery system. Response surface methodology ensures precise control over the size distribution, resulting in improved uniformity. Additionally, drug-loaded nanobubbles exhibit exceptional stability and dissolution in the gastrointestinal tract compared to traditional drug suspensions, suggesting a longer drug half-life and increased effectiveness. These findings highlight the promising role of dextran nanobubbles in ultrasound-responsive formulations for cancer therapy, offering notable benefits such as faster dissolution rates, sustained, targeted DR, and improved oral bioavailability.

FUNDING

This research received no external funding.

AUTHORS CONTRIBUTIONS

The authors conducted the study, carried out the experiments, and wrote their research plan, review, and revisions. Both authors concur in the submission and publishing. Both authors have reviewed and consented to the final version of the text for publication.

CONFLICTS OF INTERESTS

No conflict of interest

REFERENCES

1. Shibuya M. Vascular endothelial growth factor (VEGF) and its receptor (VEGFR) signaling in angiogenesis: a crucial target for anti and pro-angiogenic therapies. Genes Cancer. 2011 Dec;2(12):1097-105. doi: 10.1177/1947601911423031, PMID 22866201.
2. Raica M, Cimpean AM. Platelet-derived growth factor (PDGF)/PDGF receptors (PDGFR) axis as target for antitumor and antiangiogenic therapy. Pharmaceuticals (Basel). 2010 Mar;3(3):572-99. doi: 10.3390/ph3030572, PMID 27713269.
3. Goodman VL, Rock EP, Dagher R, Ramchandani RP, Abraham S, Gobburu JV. Approval summary: sunitinib for the treatment of imatinib refractory or intolerant gastrointestinal stromal tumors and advanced renal cell carcinoma. Clin Cancer Res. 2007 Mar;13(5):1367-73. doi: 10.1158/1078-0432.CCR-06-2328, PMID 17332278.
4. Kloth JS, Binkhorst L, DE Wit AS, DE Bruijn P, Hamberg P, Lam MH. Relationship between sunitinib pharmacokinetics and administration time: preclinical and clinical evidence. Clin Pharmacokinet. 2015 Aug;54(8):851-8. doi: 10.1007/s40262-015-0239-5, PMID 25647628.
5. Kim S, Ding W, Zhang L, Tian W, Chen S. Clinical response to sunitinib as a multitargeted tyrosine kinase inhibitor (TKI) in solid cancers: a review of clinical trials. Onco Targets Ther. 2014 May;7:719-28. doi: 10.2147/OTT.S61388, PMID 24872713.
6. Sanofi aventis US, LLC, Regeneron Pharmaceuticals Inc. Highlights of prescribing information; 2015. Available from: www.fda.gov/medwatch.
7. Lankheet NA, Kloth JS, Gadellaa Van Hooijdonk CG, Cirkel GA, Mathijssen RH, Lolkema MP. Pharmacokinetically guided sunitinib dosing: a feasibility study in patients with advanced solid tumours. Br J Cancer. 2014 May;110(10):2441-9. doi: 10.1038/bjc.2014.194, PMID 24736581.
8. Houk BE, Bello CL, Poland B, Rosen LS, Demetri GD, Motzer RJ. Relationship between exposure to sunitinib and efficacy and tolerability endpoints in patients with cancer: results of a pharmacokinetic/pharmacodynamic meta-analysis. Cancer Chemother Pharmacol. 2010 Jul;66(2):357-71. doi: 10.1007/s00280-009-1170-y, PMID 19967539.
9. Sunitinib malate solid dispersion; 2013. Available from: www.https://patents.google.com/patent/WO2013160916A1/en. [Last accessed on 28 Nov 2024].
10. Alshahrani SM, Alshetaili AS, Alalaiwe A, Alsulays BB, Anwer MK, Al Shdefat R. Anticancer efficacy of self-nanoemulsifying drug delivery system of sunitinib malate. AAPS Pharm Sci Tech. 2018 Jan;19(1):123-33. doi: 10.1208/s12249-017-0826-x, PMID 28620763.
11. Yang J, Luo L, Oh Y, Meng T, Chai G, Xia S. Sunitinib malate loaded biodegradable microspheres for the prevention of corneal neovascularization in rats. J Control Release. 2020 Nov;327:456-66. doi: 10.1016/j.jconrel.2020.08.019, PMID 32822742.

12. Sodeifian G, Razmimanesh F, Sajadian SA. Prediction of solubility of sunitinib malate (an anti-cancer drug) in supercritical carbon dioxide (SC–CO2): experimental correlations and thermodynamic modeling. J Mol Liq. 2020 Jan;297:111740. doi: 10.1016/j.molliq.2019.111740.
13. Yongvongsoontorn N, Chung JE, Gao SJ, Bae KH, Yamashita A, Tan MH. Carrier-enhanced anticancer efficacy of sunitinib loaded green tea based micellar nano complex beyond tumor-targeted delivery. ACS Nano. 2019 Jul;13(7):7591-602. doi: 10.1021/acsnano.9b00467, PMID 31262169.
14. Tarasi F, Lanza PA, Ferretti V, Echeverria GA, Piro OE, Cacicedo M. Synthesis and characterization of novel copper (II) sunitinib complex: molecular docking DFT studies hirshfeld analysis and cytotoxicity studies. Inorganics. 2014 Jul;10(1):3. doi: 10.3390/inorganics10010003.
15. Jose AD, WU Z, Thakur SS. A comprehensive update of micro and nanobubbles as theranostics in oncology. Eur J Pharm Biopharm. 2022 Mar;172:123-33. doi: 10.1016/j.ejpb.2022.02.008, PMID 35181491.
16. Kishore Kumar M, Jaya Prakash D, Basava Rao VV. Chitosan nanobubbles development and evaluation for the delivery of sunitinib an anticancer agent. Int J Appl Pharm. 2022 Jun;14(6):58-67.
17. Cavalli R, Bisazza A, Giustetto P, Civra A, Lembo D, Trotta G. Preparation and characterization of dextran nanobubbles for oxygen delivery. Int J Pharm. 2009 Nov;381(2):160-5. doi: 10.1016/j.ijpharm.2009.07.010, PMID 19616610.
18. Bessone F, Argenziano M, Grillo G, Ferrara B, Pizzimenti S, Barrera G. Low-dose curcuminoid loaded in dextran nanobubbles can prevent metastatic spreading in prostate cancer cells. Nanotechnology. 2019 May;30(21):214004. doi: 10.1088/1361-6528/aaff96, PMID 30654342.
19. Argenziano M, Banche G, Luganini A, Finesso N, Allizond V, Gulino GR. Vancomycin loaded nanobubbles: a new platform for controlled antibiotic delivery against methicillin-resistant staphylococcus aureus infections. Int J Pharm. 2017 May;523(1):176-88. doi: 10.1016/j.ijpharm.2017.03.033, PMID 28330735.
20. Sampathi S, Amancha R, Dodoala SD, Kuchana V. Biodegradable polymeric nanocarriers for oral delivery of antiretroviral drug: pharmacokinetic and *in vitro* permeability studies. J Appl Pharm Sci. 2021 Apr;11(4):28-39.
21. Rangaraj N, Pailla SR, Chowta P, Sampathi S. Fabrication of ibrutinib nanosuspension by quality by design approach: intended for enhanced oral bioavailability and diminished fast fed variability. AAPS Pharm Sci Tech. 2019;20(8):326. doi: 10.1208/s12249-019-1524-7, PMID 31659558.
22. Blanchet B, Saboureau C, Benichou AS, Billemont B, Taieb F, Ropert S. Development and validation of an HPLC-UV-visible method for sunitinib quantification in human plasma. Clin Chim Acta. 2009 Jun;404(2):134-9. doi: 10.1016/j.cca.2009.03.042, PMID 19341717.
23. Abdalkader R, Kawakami S, Unga J, Higuchi Y, Suzuki R, Maruyama K. The development of mechanically formed stable nanobubbles intended for sonoporation-mediated gene transfection. Drug Deliv. 2017 Nov;24(1):320-7. doi: 10.1080/10717544.2016.1250139, PMID 28165819.
24. Ramasundaram S, Saravanakumar G, Sobha S, OH TH. Dextran sulfate nanocarriers: design strategies and biomedical applications. Int J Mol Sci. 2022 Dec;24(1):355. doi: 10.3390/ijms24010355, PMID 36613798.
25. Batchelor DV, Armistead FJ, Ingram N, Peyman SA, McLaughlan JR, Coletta PL. The influence of nanobubble size and stability on ultrasound-enhanced drug delivery. Langmuir. 2022 Nov;38(45):13943-54. doi: 10.1021/acs.langmuir.2c02303, PMID 36322191.
26. Bhattacharjee S. DLS and zeta potential-what they are and what they are not? J Control Release. 2016 Aug;235:337-51. doi: 10.1016/j.jconrel.2016.06.017, PMID 27297779.
27. Muralikrishna P, Babu AK, Mamatha P. Formulation and optimization of ceritinib loaded nanobubbles by box-Behnken design. Int J App Pharm. 2022 Apr;14(4):219-26. doi: 10.22159/ijap.2022v14i4.44388.
28. Joseph JJ, Sangeetha D, Gomathi T. Sunitinib loaded chitosan nanoparticles formulation and its evaluation. Int J Biol Macromol. 2016 Jan;82:952-8. doi: 10.1016/j.ijbiomac.2015.10.079, PMID 26522243.
29. Gao X, Guo D, Mao X, Shan X, HE X, YU C. Perfluoropentane filled chitosan poly acrylic acid nanobubbles with high stability for long-term ultrasound imaging *in vivo*. Nanoscale. 2021 Mar;13(10):5333-43. doi: 10.1039/d0nr06878k, PMID 33659972.
30. SU C, Ren X, Nie F, LI T, LV W, LI H. Current advances in ultrasound combined nanobubbles for cancer targeted therapy: a review of the current status and future perspectives. RSC Adv. 2021 Apr;11(21):12915-28. doi: 10.1039/d0ra08727k, PMID 35423829.
31. Begum MY, Gudipati PR. Formulation and evaluation of dasatinib-loaded solid lipid nanoparticles. Int J Pharm Pharm Sci. 2018 Dec;10(12):14-20. doi: 10.22159/ijpps.2018v10i12.27567.
32. Darji AA, Bharadia PD. Chronic myelogenous leukemia: a review and update of current and future therapy. Int J Pharm Pharm Sci. 2016 Jul;8(7):35-4.
33. Anil L, Mohandas S. *In vitro* antioxidant and anticancer activity of *macranga peltata* leaf extracts on lung cancer cell lines. Int J Curr Pharm Sci. 2023 Apr;15(4):26-32. doi: 10.22159/ijcpr.2023v15i4.3019.
34. Arafath AA, Jayakar B. Enhancement of oral bioavailability via solid lipid nanoparticles of anticancer drug dasatinib an *in vitro* cytotoxicity and pharmacokinetic study. Asian J Pharm Clin Res. 2019 Jun;12(6):143-5.